PAPER

Compressional Alfvén and ion–ion hybrid waves in tokamak plasmas with two ion species

IOP Publishing Plasma Physics and Controlled Fusion

Plasma Phys. Control. Fusion **56** (2014) 125017 (9pp) doi:10.1088/0741-3335/56/12/125017

Compressional Alfvén and ion–ion hybrid waves in tokamak plasmas with two ion species

H J C Oliver[1,2], S E Sharapov[2], R Akers[2], I Klimek[3], M Cecconello[3] and the MAST Team[2]

[1] H H Wills Physics Laboratory, University of Bristol, Royal Fort, Tyndall Avenue, Bristol BS8 1TL, UK
[2] CCFE, Culham Science Centre, Abingdon, Oxfordshire OX14 3DB, UK
[3] Department of Physics and Astronomy, Uppsala University, SE-751 05 Uppsala, Sweden

E-mail: James.Oliver.2011@my.bristol.ac.uk

Received 2 July 2014, revised 17 October 2014
Accepted for publication 28 October 2014
Published 17 November 2014

Abstract

Compressional Alfvén and ion–ion hybrid waves excited by energetic beam ions are studied in plasmas with two ion species. In our experiment, a hydrogen-deuterium (H-D) plasma is used to produce instabilities similar to those likely to be present in the burning deuterium-tritium plasmas of future tokamaks. Modes are suppressed in the deuterium cyclotron frequency range with increasing hydrogen gas puffing. In plasmas with H/D concentrations of 2.57 or higher, short-lived modes with small and predominantly negative toroidal mode numbers are observed at frequencies $\omega/\omega_{\beta D0} \approx 2.25$, where $\omega_{\beta D0} = \omega_{\beta D}(R_0)$ is the on-axis deuterium cyclotron frequency. These are the highest mode frequencies yet detected in the ion cyclotron range in a spherical tokamak. Modeling of the transparency regions and plasma resonances using the cold plasma dispersion relation explains the observed features. Mode conversion at ion–ion hybrid resonances and subsequent kinetic damping is believed to be responsible for mode suppression. The high frequency modes are present due to excitation by wave-particle resonances within the transparency region for high hydrogen concentrations. The absence of other wave-particle resonances explains significant features of our experiment. This technique has possible applications in plasma heating, current drive and real-time diagnosis of relative ion concentration in the plasma core.

Keywords: alfven waves, tokamaks, multi-component and negative-ion waves

(Some figures may appear in colour only in the online journal)

1. Introduction

Compressional Alfvén (or fast magnetosonic) waves driven unstable by super-Alfvénic energetic deuterium beam ions have previously been detected in deuterium plasmas in the Mega Ampere Spherical Tokamak (MAST) at frequencies from $0.1 \leqslant \omega/\omega_{\beta D0} \leqslant 1.4$ [1–3], where $\omega_{\beta D0} = \omega_{\beta D}(R_0)$ is the on-axis deuterium cyclotron frequency. They have also been seen in many other machines including the spherical tokamaks START [4] and NSTX [5] and the 'conventional' tokamak DIII-D [6].

Compressional Alfvén Eigenmodes (CAEs) have been the subject of extensive study due to their potential ability to affect beam current drive and transfer energy from fast ions—either fusion products in burning plasmas, ions accelerated by Ion Cyclotron Resonance Heating (ICRH) or ionised Neutral Beam Injection (NBI) beam particles—to thermal plasma ions in future tokamak reactors.

Plasma resonances and cut-offs of externally launched radio frequency waves have been exploited to diagnose relative ion concentrations in hydrogen-deuterium plasmas [7]. This technique was further explored theoretically for determining the deuterium-tritium (D-T) mixture of a plasma in a future spherical tokamak power planet using radio frequency waves [8].

In plasmas with two ion species of unequal charge/mass ratio—for example, in the D-T plasmas of future tokamak reactors—CAEs transform into ion–ion hybrid waves at frequencies between the two ion cyclotron frequencies [9]. In section 2 of this paper, we present the results of a recent MAST experiment in which hydrogen ions were used in addition to deuterium ions to produce Alfvén instabilities similar to those likely to be present in burning tokamak plasmas. In section 3 the cold plasma approximation is applied to find a wave dispersion equation with notable consequences of the equation discussed. In section 4 the theory of section 3 is used to model the transparency regions of modes to explain the experimental observations presented in section 2. In section 5 the possible applications of the technique are discussed. Finally, section 6 presents the conclusions of our findings.

2. Experimental observations

The initial discharges of the experiment consisted of pure deuterium plasmas to establish a reference scenario with strong CAE activity up to frequencies $\omega/\omega_{\beta D0} > 1$. Waves were detected by the OMAHA coil array [10] with a sampling rate of 10 MHz, limiting detection of wave-induced edge magnetic perturbations to a Nyquist frequency of 5 MHz ($\geqslant 2\omega_{\beta D0} = \omega_{\beta H0}$, the on-axis proton cyclotron frequency). Therefore a low toroidal magnetic field ($B_T \approx 0.3$ T) was required to ensure the proton cyclotron frequency was less than 5 MHz.

All discharges in the experiment followed the same scenario with typical plasma characteristics: Plasma current $I \approx 600$ kA. The toroidal on-axis magnetic field, B_T, decreased from 0.38 T at 50 ms before stabilizing at $B \approx 0.3$ T at 100 ms. The on-axis electron density $n_e(R_0) \approx 2 \times 10^{19}$ m^{-3}, on-axis electron temperature $T_e(R_0) \approx 800$ eV, with the electron density and temperature profiles measured by Thomson scattering diagnostics with high radial resolution. Heating is provided by one deuterium on-axis neutral beam delivering a total power $P_{NBI} \approx 2$ MW with most particles injected with a kinetic energy of $E_b = 70$–74 keV. This particle energy corresponds to a beam particle velocity $v_b \approx 2.6 \times 10^6$ ms^{-1}, larger than the Alfvén velocity $V_A = B/\sqrt{\mu_0 \rho_i} \sim 10^6$ ms^{-1}. Therefore the beam was super-Alfvénic.

Toroidal mode numbers of the modes were calculated using toroidally separated OMAHA coils to assess the toroidal phase shifts of the mode. Negative toroidal mode numbers denote phase velocity in the counter-NBI/counter-current/co-magnetic field direction, i.e. the opposite direction to modes with positive toroidal mode numbers.

In the reference scenarios, perturbations with toroidal mode numbers up to $n = 17$ were observed at frequencies of $\omega/\omega_{\beta D0} \approx 1.4$ and down to $n = -7$ at frequencies of $\omega/\omega_{\beta D0} \approx 0.15$. Modes with small positive toroidal mode numbers ($1 \leqslant n \leqslant 4$) were weakly excited. Gradually the H/D concentration (n_H/n_D) was increased between discharges by introducing increasingly long puffs of hydrogen gas from the low field side of the tokamak. The hydrogen puff timings are shown in table 1. Outside of hydrogen gas puffing, the plasma was refueled with deuterium gas puffing from the high field side.

Table 1. Duration of hydrogen gas puff for the presented MAST discharges.

Plasma discharge	Start time of hydrogen puff (ms)	End time of hydrogen puff (ms)
30080	0	0
30457	0	0
30463	0	100
30468	40	180 (end of discharge)
30471	0	180 (end of discharge)

The H : D relative concentrations were determined using simulations obtained from TRANSP [11], a global transport analysis code, to find the H/D concentration most closely matching the neutron yield measured by a U-235 fission chamber [12]. The presence of hydrogen dilutes the deuterium content of the bulk plasma, thereby reducing the D–D neutron rate.

As more hydrogen was introduced into the plasma, the amplitude of the Compressional Alfvén and ion–ion hybrid waves (observed at frequencies greater than 400 kHz) decreased until the modes were entirely suppressed in the ion cyclotron frequency range, as shown in figure 1. Toroidal Alfvén Eigenmodes (TAEs) are observed at frequencies less than 250 kHz throughout the experiment regardless of H/D relative concentration.

At the highest H/D concentrations investigated, short-lived modes unlike CAEs previously seen in deuterium plasmas were detected at very high frequencies ($\sim \omega_{\beta H0}$), shown in figure 2. The toroidal mode numbers of these perturbations were small ($|n| \leqslant 3$) and mostly negative. The highest frequency mode observed in this experiment was detected at $\omega/\omega_{\beta D0} = 2.25$, shown in figure 3. The discharges during which magnetic activity at the highest frequency was observed had similar characteristics to those of the other plasma discharges in the experiment (presented above), except for plasma density which was lower, $n_e(R_0) \approx 1.5 \times 10^{19}$ m^{-3}, due to the differences in gas puffing efficiency for hydrogen and deuterium.

The mismatch between measured and simulated neutron rates presented in figure 4 suggests that the H/D concentration fluctuated during excitation of the high frequency modes ($0.1 \leqslant$ t(s) $\leqslant 0.112$) in discharge #30471, but was greater than 2.57 while the high frequency modes were excited. No TRANSP modeling was possible for the other discharges with high frequency modes, but the H/D concentrations are likely to be similar due to the consistency of experimental parameters and the high reproducibility of MAST discharges.

The plasma was scanned radially with a mobile neutron camera [13] over a series of identical discharges to observe how the neutron flux and hence relative ion concentration, varied as a function of radius [12]. No significant change was observed in the radial DD neutron count rate profile within experimental uncertainties. Hence we conclude that the relative ion concentration is constant with radius.

Modes in the frequency range $0.2 \leqslant \omega/\omega_{\beta D0} \leqslant 0.5$, which mostly have negative toroidal mode numbers, were

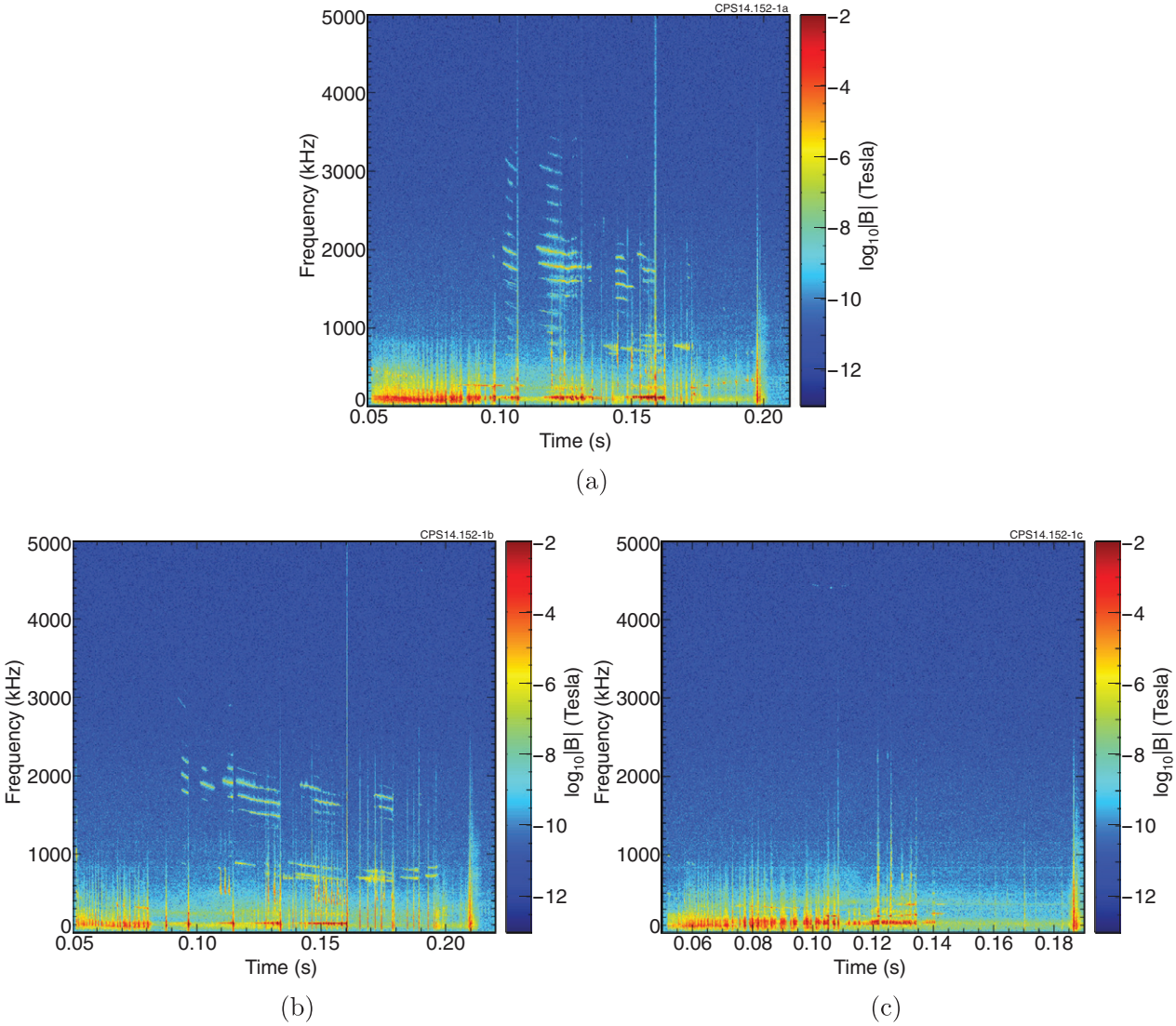

Figure 1. Magnetic spectrographs showing the logarithm of the amplitude of magnetic perturbations normalised to the equilibrium magnetic field excited in MAST discharges: (*a*) #30457, (*b*) #30463 and (*c*) #30471. Hydrogen puffing duration increases as: (*a*) 0 ms (reference scenario), (*b*) 100 ms, (*c*) 180 ms.

excited in all discharges except those with the highest concentrations of hydrogen. The modes in this frequency range mostly had toroidal mode numbers $n = -6$ and -7 (pink and yellow in figure 5).

In previous MAST experiments optimised for exciting CAEs, modes with toroidal mode numbers that were negative and had magnitudes of $|n| \geqslant 4 - 6$ were also dominant in this frequency range [1, 2, 14].

3. Theory

It has been shown that tokamak plasmas with β of order unity have approximately one dimensional equilibria in the core [15]. Additionally the geometry of a highly elliptical plasma causes the equilibrium to be approximately 1D. For the plasmas considered, the ratio of plasma height to width is ∼1.65–2 and $\beta \sim 0.1$. As MAST operates with both highly elliptical plasmas and moderate values of β, the idealisation of a 1D equilibrium, known as a 'hollow cylinder' approximation, is approximately applicable. Therefore the density profile and magnetic field configuration are functions only of radius as there is only a relatively small variation of parameters in the vertical direction.

3.1. Dielectric tensor

The cold plasma dielectric tensor ε describes the dielectric response of the plasma to a perturbation [16]:

$$\varepsilon = \begin{pmatrix} \varepsilon_1 & i\varepsilon_2 & 0 \\ -i\varepsilon_2 & \varepsilon_1 & 0 \\ 0 & 0 & \varepsilon_3 \end{pmatrix} \quad (1)$$

Where:

$$\varepsilon_1 = 1 - \sum_\alpha \frac{\omega_{p\alpha}^2}{\omega^2 - \omega_{\beta\alpha}^2}$$

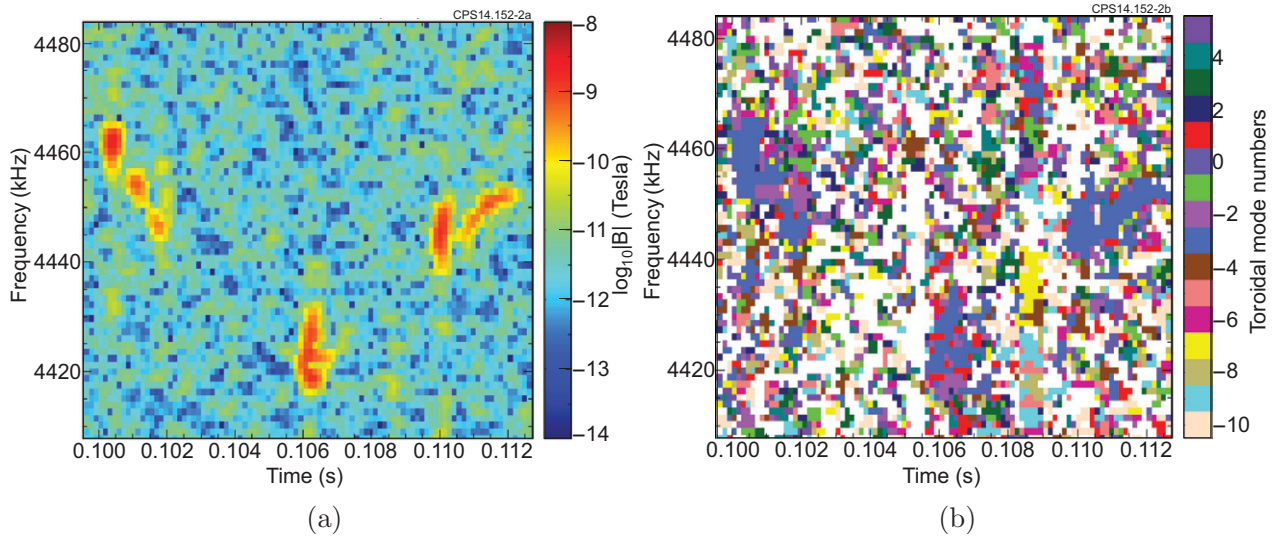

Figure 2. (*a*) Magnetic spectrograph showing the amplitude of magnetic perturbations for discharge #30471 at a time when high frequency modes were present. (*b*) Phase magnetic spectrograph showing toroidal mode numbers ($n = -3$ primarily) of the modes excited.

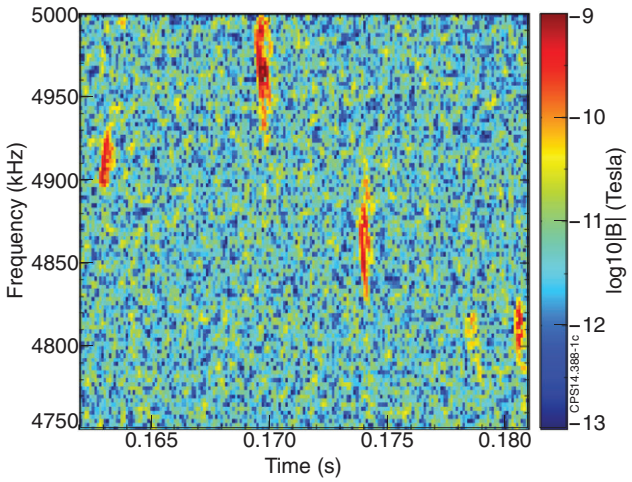

Figure 3. Magnetic spectrograph showing the amplitude of magnetic perturbations for discharge #30468 at a time when high frequency modes were present.

$$\varepsilon_2 = -\sum_{\alpha} \frac{\omega_{\beta\alpha}\omega_{p\alpha}^2}{\omega(\omega^2 - \omega_{\beta\alpha}^2)}$$

$$\varepsilon_3 = 1 - \sum_{\alpha} \frac{\omega_{p\alpha}^2}{\omega^2}$$

$\omega_{\beta\alpha}(R) = q_\alpha B(R)/m_\alpha$ and $\omega_{p\alpha}(R) = \left(n_\alpha(R)\, q_\alpha^2 / m_\alpha \varepsilon_0\right)^{\frac{1}{2}}$ are the cyclotron and plasma frequencies of species $\alpha = \{H, D, e\}$ with charge q_α and mass m_α. In this co-ordinate system the local magnetic field B is in the z direction and the wave vector $\mathbf{k} = (k_\perp, 0, k_\parallel)$. The limitations of the cold plasma approximation are discussed in section 3.3.

3.2. Cold plasma dispersion relation

From Faraday's and Ampère's Laws a general wave equation for the perturbed electric field **E** can be derived by decomposing the wave fields and perturbed current

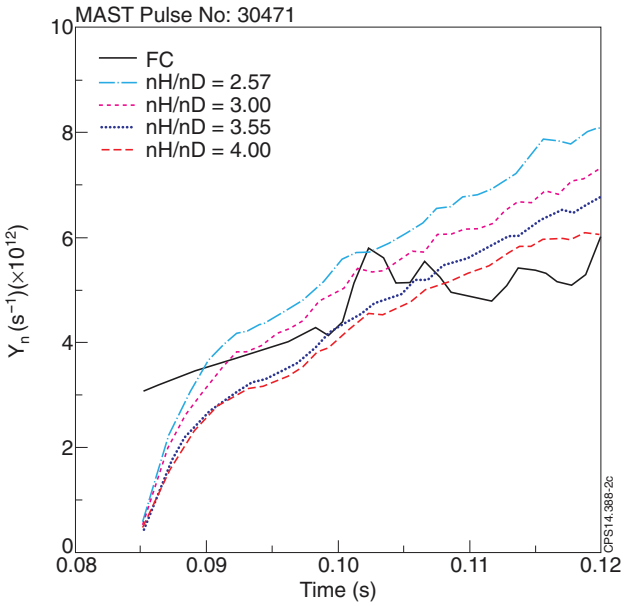

Figure 4. Neutron yield Y_n measured by a fission chamber against neutron yields predicted by TRANSP for different hydrogen-deuterium ratios.

density **j** into Fourier components of the form $\{\boldsymbol{B}, \boldsymbol{E}, \boldsymbol{j}\} = \{\boldsymbol{B_0}, \boldsymbol{E_0}, \boldsymbol{j_0}\}\exp[\mathrm{i}(\mathbf{k}\cdot\mathbf{r} - \omega\, t)]$:

$$-\mathbf{k}\times\mathbf{k}\times\mathbf{E} - \left(\frac{\omega}{c}\right)^2 \mathbf{E} = \mathrm{i}\omega\mu_0 \sum_{\alpha} \mathbf{j_\alpha} \qquad (2)$$

The conductivity tensor σ relates the current density and electric field: $j_{\alpha i} = \sigma_{ij}^{(\alpha)} E_j$. The dielectric tensor is given by: $\varepsilon_{ij} = \delta_{ij} + \sum_\alpha \frac{\mathrm{i}}{\omega\varepsilon_0}\sigma_{ij}^{(\alpha)}$, where δ_{ij} is the contribution from the vacuum given by the unit matrix [17]. From these two definitions equation (2) can be written:

$$\left[N^2\left(\frac{k_i k_j}{k^2} - \delta_{ij}\right) + \varepsilon_{ij}\right] E_j = 0 \qquad (3)$$

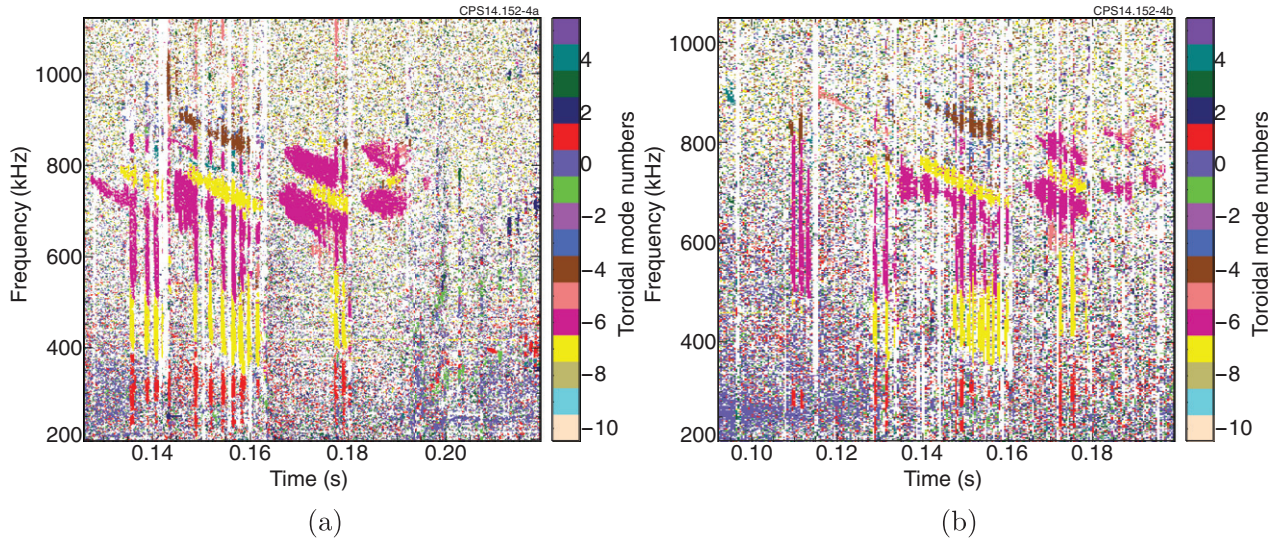

Figure 5. Phase magnetic spectrograph showing toroidal mode numbers of the modes excited in the negative toroidal mode frequency range for discharges (*a*) #30080 and (*b*) #30463.

Where $N^2 = N_\parallel^2 + N_\perp^2 = \left(\frac{ck_\parallel}{\omega}\right)^2 + \left(\frac{ck_R}{\omega}\right)^2$ is the square of the refractive index and there is an implied summation over the j index.

By setting the determinant of the matrix represented by the coefficients of E_j in equation (3) equal to zero and by the taking limit $\varepsilon_3 \to \infty$ for perfect conductivity (the parallel perturbed electric field $E_\parallel \to 0$), one obtains an equation for the perpendicular refractive index $N_\perp$:

$$N_\perp^2 = \varepsilon_1 - N_\parallel^2 - \frac{\varepsilon_2^2}{\varepsilon_1 - N_\parallel^2} \tag{4}$$

As a tokamak plasma is inhomogeneous with a $1/R$ magnetic field configuration, the dielectric tensor elements and therefore $N_\perp^2$, will vary radially. When $N_\perp^2 = 0$ a wave is reflected except for an evanescent tail that is transmitted and decays exponentially [17]. The reflection points cause a wave to be localised in a region of positive $N_\perp^2$ called a 'transparency region'. If there is sufficient drive within this region a wave can be excited via the wave-particle resonance, which is described by the wave-particle resonance condition [1]:

$$\omega = \left(k_\parallel + \frac{s}{qR_0}\right) v_\parallel + p\omega_{\beta b} \tag{5}$$

Where s is an integer, q is the safety factor and $\omega_{\beta b}$ is the beam species cyclotron frequency. The quantity p is an integer denoting the type of resonance under consideration. $p = -1$ represents the anomalous Doppler resonance, which is valid for modes with positive toroidal mode numbers. $p = +1$ represents the normal Doppler resonance, which applies for modes with negative toroidal mode numbers. The $s/q\,R_0$ correction to equation (5) applies for passing resonant particles in circular flux surfaces. While the latter condition isn't strictly accurate for MAST plasmas, it has only a small effect on the position of the resonances in this application.

3.3. Resonances

From equation (4) one can see there will be a singularity in $N_\perp^2$ at any point in the plasma for which $\varepsilon_1 = N_\parallel^2$. For plasmas with one ion species this singularity is known as the Alfvén resonance. When a second species is introduced another resonance, known as the ion–ion hybrid resonance, appears at frequencies between the two ion cyclotron frequencies. For the cold plasma approximation to hold, the ion–ion hybrid resonances must not occur too close to the proton cyclotron frequency to avoid cyclotron resonances. This restricts the use of this model for $\kappa_H = n_H / n_e < 2v_{TD}^2 / V_A^2$ [18] where v_{TD} is the thermal velocity of deuterium. Hence the model may not apply for $0 < \kappa_H \lesssim 0.15$. This limitation does not restrict this work as the hydrogen concentrations of interest in this article are either below (i.e. pure D) or above this limit.

As a singularity is approached the perpendicular wavelength of the wave $\lambda_\perp$ decreases as $k_\perp \to \infty$. Once $\lambda_\perp$ decreases to values comparable to the ion Larmor radius ρ_i the cold plasma approximation is no longer applicable. The inclusion of thermal effects causes the singularity to be resolved by the appearance of a short wavelength wave to which energy transfers from the incident wave at the position of the resonance [19]. The incident wave converts into a kinetic Alfvén wave for $\omega/\omega_{\beta D0} < 1$ and into an ion Bernstein wave for $\omega/\omega_{\beta D0} > 1$ [17].

Kinetic damping dissipates the wave for $\lambda_\perp \sim \rho_i$ [20] and so both the kinetic Alfvén and ion Bernstein waves are heavily damped. The $\varepsilon_1 = N_\parallel^2$ resonance is one of the most significant damping mechanisms for Compressional Alfvén and ion–ion hybrid waves [8].

When a wave reflects at a cut-off, an evanescent tail can tunnel through a region of negative $N_\perp^2$ to a resonance whereupon the wave is mode converted and damped heavily. As a result a wave propagating in a transparency region with a resonance close to one or both of the reflection points will be damped at a rate [8] related to the sum of the exponentials of

the radial distance of the singularities to the reflection points normalised to the minor radius a.

Previous studies have found that the absorption rate of the Compressional Alfvén wave from mode conversion and subsequent damping is high enough during a single wave cycle, referred to as the fractional dissipation rate, that up to 90% of the wave power can be dissipated over a few passes [21]. Additionally, it has been found that a range of dissipation mechanisms can easily satisfy the condition: fractional dissipation rate $\sim\rho_i/a$. This ensures the mode-converted short wavelength wave is entirely dissipated in the plasma [20].

3.4. Wave frequency quantisation

For a wave localised between two reflection points, a discrete spectrum of modes each with a different radial mode number l is found from the quantisation condition [22]:

$$\int_{R_1}^{R_2} k_R(R,\omega)dR \simeq \frac{\omega}{c}\int_{R_1}^{R_2} N_\perp(R,\omega)dR = \pi\left(l+\frac{1}{2}\right) \qquad (6)$$

Equation (6) can be used in conjunction with equation (4) to determine the frequencies at which modes can propagate within the transparency region for a given radial mode number, with $R_{1,2}$ representing the reflection points. By scanning over frequency and integrating $N_\perp$ over the transparency region, the radial mode number can be determined for each frequency. Integer radial mode numbers are obtained for the allowed frequencies.

4. Modeling of wave transparency regions and plasma resonances

Equation (4) was used to plot the perpendicular refractive index squared $N_\perp^2$ profile for a given wave frequency ω, parallel wave number $k_\parallel \approx n/R_0$ and relative ion concentration:

$$\kappa_D = n_D/n_e = 1-\kappa_H \qquad (7)$$

The density profile and equilibrium data for figures 6–8 correspond to MAST shot #30463 at $t = 124$ ms. Figure 6 shows an example of a $N_\perp^2$ profile with reflection points located at $r = 1.05$ m and 1.41 m, two ion–ion hybrid resonances located at $r = 1.01$ m and 1.46 m and an Alfvén resonance located at $r = 0.47$ m (the other Alfvén resonance has moved out of the plasma on the low field side). In this section, the theory presented in section 3 is used to explain the phenomena observed in section 2.

4.1. Explanation of the suppression of modes

Varying ω and κ_D causes the $N_\perp^2$ profile and therefore the reflection points and resonance positions, to change. Following theory discussed in section 3.3, for each point in $\omega-\kappa_D$ parameter space a measure of the damping of the wave due to mode conversion is given by $\Sigma_{c,s}\exp(-|(r_c-r_s)/a|)$, where subscript c denotes the reflection points and subscript s denotes the plasma resonances. The distance between the position of

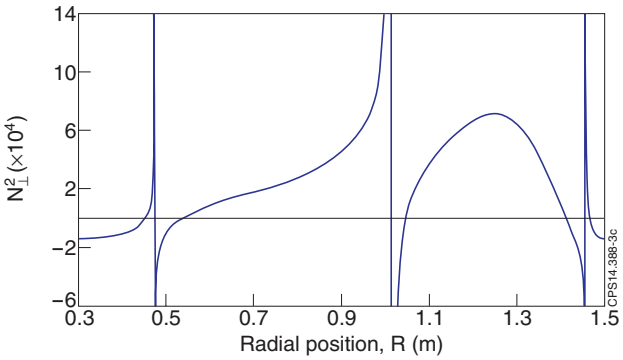

Figure 6. $N_\perp^2$ profile plotted using data corresponding to MAST shot #30463 at $t = 124$ ms with $\omega/\omega_{\beta D0} = 1.1$, $n = \pm 6$ and $\kappa_D = 0.25$.

the reflection point r_c and the resonance r_s is normalised to the plasma minor radius a.

Schematic examples are shown in figure 7 for $n = \pm 2$ and $n = \pm 6$. Blue represents a lack of damping—the measure of damping is equal to 0—where no resonances are present. Red represents a relatively high rate of damping, which occurs when the measure of damping ≈2 as a resonance is near each of the reflection points. Green represents a relatively low rate of damping, which occurs when the measure of damping ≈1, i.e. when only one resonance is close to a reflection point—usually when the other resonance of the pair has moved out of the plasma on the low field side.

In order to be significant, strongly-damped modes require strong drive. In these MAST plasmas, a strong source of instability drive exists due to positive velocity and spatial gradients of the beam ion distribution, an example of which is shown later. In the two limiting cases $\kappa_D = 1$ (pure deuterium) and $\kappa_D = 0$ (pure hydrogen), one can see the frequency below which strong wave damping by the Alfvén resonance occurs changes by a factor of two, as the ion cyclotron frequency also changes by the same factor.

With increasing H/D concentrations (κ_H/κ_D), the mode is damped over a wider range of frequencies in the deuterium cyclotron frequency range. This result could explain the suppression of modes with increased hydrogen puffing observed in our experiment (see figure 1).

4.2. Explanation of the dominance of n = – 6, –7 modes at low frequencies

Figure 7 shows modes with small toroidal mode numbers are relatively strongly damped in the frequency range usually associated with negative toroidal mode numbers. The frequency range of the strong damping decreases with increasing toroidal mode number. This observation was investigated further using equation (6) to find the lowest allowed wavelengths for a given toroidal mode number. The lowest allowed wave frequency, which corresponds to the lowest energy oscillation, occurs for radial mode number $l = 0$. In figure 8 the relevant frequency range of mode damping is plotted against parallel wavenumber $k_\parallel \approx n/R_0$ for a pure deuterium plasma, which has the widest frequency range of heavy damping. Waves with

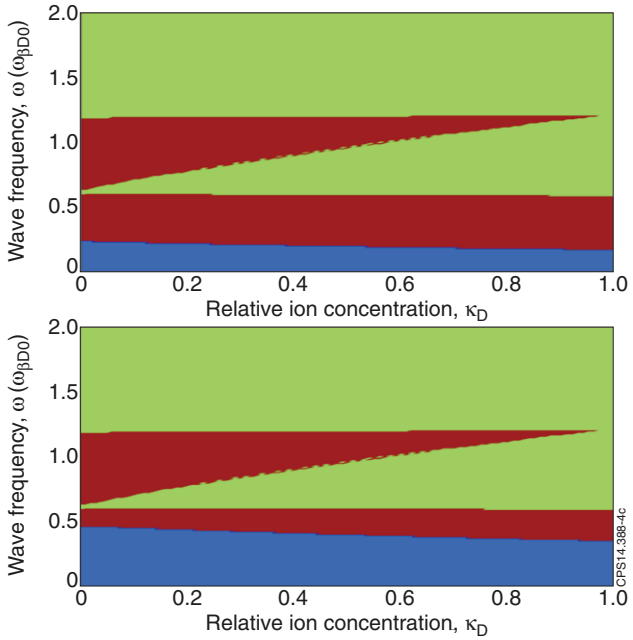

Figure 7. Schematic of the damping of modes with frequency ω in plasmas with relative ion concentration κ_D. Blue represents no damping, green represents a relatively low rate of damping and red represents a relatively high rate of damping. Top: $n = \pm 2$; bottom: $n = \pm 6$.

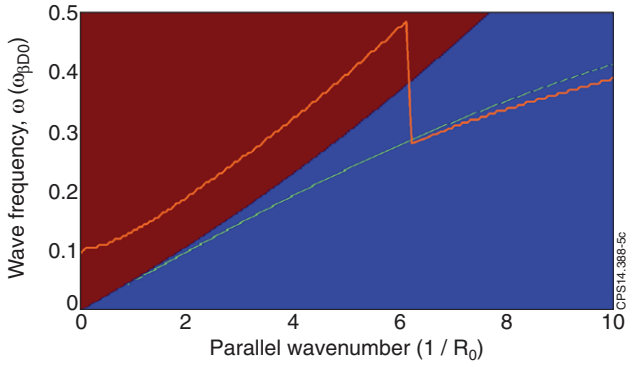

Figure 8. A measure of damping for modes with different parallel wavenumbers for $\kappa_D = 1$. Blue (bottom right) represents no damping, green represents a relatively low rate of damping and red (top left) represents a relatively high rate of damping. Overlaid in orange is the lowest allowed frequency.

toroidal mode numbers $|n| < 6$ are strongly damped in the frequency range associated with modes with negative toroidal mode numbers. This result agrees with features observed in the hydrogen-deuterium experiment (see figure 5), where the excited modes in this frequency range mainly had $n = -6, -7$.

4.3. Explanation of the presence of high frequency modes with increasing hydrogen concentrations

As a necessary condition for wave existence, the existence of wave-particle resonances inside the transparency region was investigated by applying equation (5) to find the position of the resonance for a given wave frequency and integer s. By

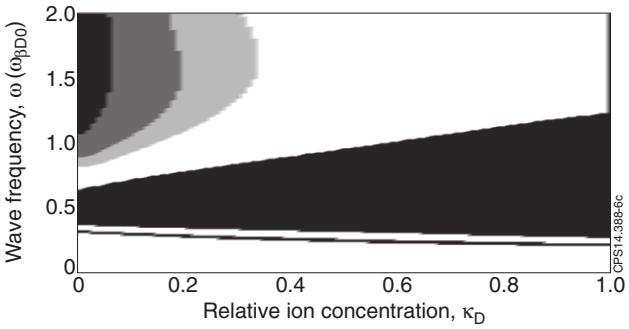

Figure 9. Existence of a resonance for each point in the relevant $\omega - \kappa_D$ parameter space for a mode with $n = -3$. Black represents the $s = 4$ resonance, dark grey represents the $s = 5$ resonance, light grey represents the $s = 6$ resonance and white denotes an absence of any significant resonance.

calculating the $N_\perp^2$ profile for a possible mode at each point in $\omega - \kappa_D$ parameter space the transparency regions can be found. The existence of a resonance within the transparency region for a mode with toroidal mode number $n = -3$ (a typical toroidal mode number for the high frequency modes) is shown in figure 9. This was modeled using the equilibrium data and density corresponding to MAST discharge #30471 at the time at which high frequency mode excitation first began ($t = 100$ ms).

For waves with high frequencies and small negative toroidal mode numbers a wave-particle resonance exists inside the transparency region in plasmas with high hydrogen concentrations. This result agrees with the experimental observation of high frequency modes in high hydrogen plasmas (see figure 2). The H/D concentration was greater than 2.57 during high frequency mode excitation (see figure 4). The high frequency modes were first excited at $\omega/\omega_{\beta D0} = 1.93$ corresponding to a theoretical critical H/D concentration of 2.25 from figure 9. Hence good agreement is found between the theoretical and experimental results. Due to the high s number, the wave-particle resonance is weaker and hence the perturbation will have a lower amplitude. This is consistent with the observation that the mode amplitude δB (see figure 2) is up to $\sim 10^4$ smaller than typical CAE amplitudes.

The existence of a wave-particle resonance within the transparency region is only significant if a free energy source of fast particles exists from which energy can be transferred to drive the wave. To check such a free energy source exists, LOCUST [23], a fast ion Monte Carlo code, was run to check for positive gradients in the velocity space distribution function of fast ions, which are required to drive the mode unstable [5]. LOCUST discards thermalised fast ions. Large positive velocity gradients are observed in the beam ion distribution function, an example of which is shown in figure 10.

A positive gradient or 'bump-on-tail' exists at $-0.4 \lesssim V_\#/V_{\text{norm}} \lesssim -0.1$ and $-0.95 \lesssim V_\#/V_{\text{norm}} \lesssim -0.85$, where $V_\#/V_{\text{norm}}$ is the particle velocity parallel to the equilibrium magnetic field normalised to the maximum injection velocity, for particles moving almost parallel to the equilibrium magnetic field, $V_\xi/V_{\text{norm}} \approx 0$. The bump-on-tails are formed due to the velocity space anisotropy of the injected

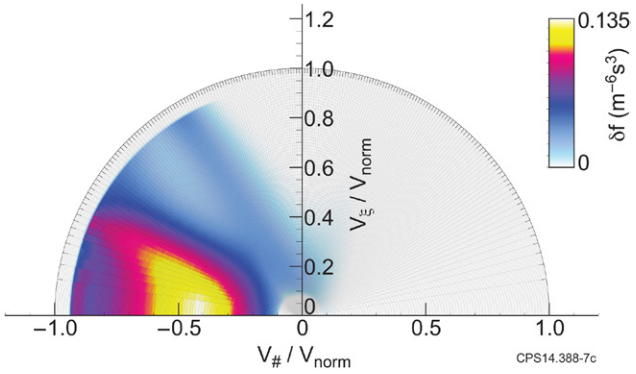

Figure 10. An example of the existence of positive gradients in the NBI ion distribution function on the mid-plane at $R = 1.186$ m for MAST discharge #30471 at time $t = 100$ ms. The colour bar represents the number of fast particles per unit velocity space per unit space, δf (m^{-6} s^3). V_ξ, the particle velocity perpendicular to the equilibrium magnetic field and $V_\#$, the particle velocity parallel to the equilibrium magnetic field, are both normalised to the maximum injection velocity, V_{norm}.

beam ions. The positive velocity gradients will strongly drive the mode instability.

4.4. Explanation of toroidal mode number limits

The presence of wave-particle resonances within transparency regions was assessed for simulations using equilibrium data corresponding to a range of discharges. No resonances were found within the transparency regions for modes with toroidal mode numbers $n > 17$ and $n < -7$. This explains the range of toroidal mode numbers observed. Furthermore, the transparency region for modes with $n = 1, 2, 3, 4$ only contain resonances with $s \geqslant 6, 5, 4, 3$ respectively. This suggests the magnetic perturbations with these mode numbers were weak because the modes were only able to access the free energy source of fast particles through weak resonances.

5. Applications

Observations of excited modes used in conjunction with transparency region simulations could provide a novel diagnostic for relative ion concentrations in the core using only standard magnetic diagnostics. First the frequency and toroidal mode numbers of any excited waves must be observed and plasma density and equilibrium magnetic field measured. By simulating the transparency region and resonances of a hypothetical mode, the relative ion concentration can be diagnosed at the position of wave excitation. Due to the low computational intensity this procedure could be carried out in seconds to provide approximate real-time ion concentrations that are crucial for optimisation of fusion efficiency in a burning plasma core.

The positions of the plasma resonances can be established using the measured data in conjunction with equation (4). The existence of wave-particle resonances within the transparency region can be checked using equations (4) and (5). Targeting NBI or ICRH at a wave-particle resonance within a transparency region with a plasma resonance close to at least one reflection point will efficiently heat the plasma by the process described in section 3.3. Mode conversion at plasma resonances can also drive current in the plasma [21].

However, the measure of mode damping described in this paper is a qualitative description of a complex phenomenon. To calculate the damping rates a full wave treatment is required. Whilst computationally intensive, this method would allow calculation of the rate of plasma heating by wave absorption. A full treatment would need to account for interference between reflected and incoming waves near reflection points as well as refraction of the wave.

6. Conclusions

In conclusion, during our experiment in which hydrogen puffing duration was gradually increased, modes were suppressed in the deuterium cyclotron frequency range. Modes were excited with small negative toroidal mode numbers at frequencies near the proton cyclotron frequency for plasmas with H/D concentrations of greater than 2.57. Negative toroidal mode numbers $n < 0$ denote propagation in the counter-current/counter-beam direction.

Transparency region and plasma resonance analysis using the cold plasma dispersion relation can explain the observed mode activity. Mode conversion and damping causes the mode suppression with increasing hydrogen puffing. Similar suppression of CAEs is expected between the two ion cyclotron frequencies for D-T plasma. The high frequency modes exist due to wave-particle resonances within the plasma transparency region, which is modified by the H/D mix, for high hydrogen concentrations. The experimental H/D concentration in such cases is in agreement with the theoretical critical concentration. For frequencies $\omega/\omega_{\beta D0} \leqslant 0.5$, the most strongly excited modes have negative toroidal mode numbers $n = -6, -7$. Modes with lower absolute values of n (but still with $n < 0$) are subject to strong damping. Modes with toroidal mode numbers $n \leqslant -8$ are suppressed due to an absence of wave-particle resonances inside the transparency region. The range of CAEs excited in the reference scenario discharges is limited for the same reason. Modes with $1 \leqslant n \leqslant 4$ are weakly excited as only higher order wave-particle resonances are accessible. The technique presented in this paper has possible applications in tokamak operations for plasma heating, current drive and ion concentration diagnosis in the core.

Acknowledgments

The authors thank Matt Lilley and Michael Fitzgerald for inspiring discussions and Ken McClements for support in the preparation of this manuscript.

This project has received funding from the European Union's Horizon 2020 research and innovation programme under grant agreement number 633053 and from the RCUK Energy Programme (grant number EP/I501045). To obtain further information on the data and models underlying this paper please contact PublicationsManager@ccfe.ac.uk. The views and opinions expressed herein do not necessarily reflect those of the European Commission.

References

[1] Sharapov S E, Lilley M K, Akers R, Ben Ayed N, Cecconello M, Cook J W C, Cunningham G, Verwichte E and the MAST Team 2014 Bi-directional alfvén cyclotron instabilities in spherical tokamak MAST *Phys. Plasmas* **21** 082501

[2] Appel L C, Fülöp T, Hole M J, Smith H M, Pinches S D, Vann R G L and The MAST Team 2008 Compressional alfvén eigenmodes on MAST *Plasma Phys. Control. Fusion* **50** 115011

[3] Gryaznevich M P *et al* 2008 Recent experiments on alfvén eigenmodes in MAST *Nucl. Fusion* **48** 084003

[4] McClements K G, Gryaznevich M P, Sharapov S E, Akers R J, Appel L C, Counsell G F, Roach C M and Majeski R 1999 Physics of energetic particle-driven instabilities in the START spherical tokamak *Plasma Phys. Control. Fusion* **41** 661

[5] Fredrickson E D *et al* 2001 Observation of compressional alfvén modes during neutral-beam heating on the national spherical torus experiment *Phys. Rev. Lett.* **87** 145001

[6] Heidbrink W W, Fredrickson E D, Gorelenkov N N, Rhodes T L and Van Zeeland M A 2006 Observation of compressional alfvén eigenmodes (CAE) in a conventional tokamak *Nucl. Fusion* **46** 324

[7] Watson G W, Heidbrink W W, Burrell K H and Kramer G J 2004 Plasma species mix diagnostic using ion–ion hybrid layer reflectometry *Plasma Phys. Control. Fusion* **46** 471

[8] Lilley M K and Sharapov S E 2007 Compressional alfvén and ion–ion hybrid modes in the deuterium-tritium plasma of a spherical tokamak power plant *Phys. Plasmas* **14** 082501

[9] Lilley M K 2009 Resonant interaction of fast particles with alfvén waves in spherical tokamaks *PhD Thesis* Imperial College, London

[10] Hole M J and Appel L C 2003 A Novel Technique for Eigenmode Analysis *30th EPS Conf. on Controlled Fusion and Plasma Physics* (*St Petersburg*, 7–11 July, 2003) ECA vol 27A, p 3132

[11] Budny R V 1994 A standard DT supershot simulation *Nucl. Fusion* **34** 1247

[12] Klimek I, Cecconello M, Sharapov S E, Harrison J and Ericsson G 2014 Determination of hydrogen/deuterium ratio with neutron measurements on MAST *Rev. Sci. Instrum.* **85** 11E109

[13] Cecconello M *et al* 2014 The 2.5 MeV neutron flux monitor for MAST *Nucl. Instrum. Methods Phys. Res.* A **753** 72

[14] Lilley M K, Sharapov S E, Smith H M, Akers R J, McCune D and MAST Team 2008 Modelling of beam-driven high frequency alfvén eigenmodes in MAST *Proc. of 35th EPS Conf. on Plasma Physics* (*Hersonissos*, 9–13 June 2008) ECA vol 32D, p 1057

[15] Hsu S C, Artun M and Cowley S C 1996 Calculation and interpretation of analytic high-beta poloidal equilibria in finite aspect ratio tokamaks *Phys. Plasmas* **3** 266

[16] Akhiezer A I *et al* 1975 *Plasma Electrodynamics Volume 1: Linear Theory* 1st edn (Oxford: Pergamon Press)

[17] Stix T H 1992 *Waves in Plasmas* (New York: American Institute of Physics)

[18] Wesson J 2004 *Tokamaks* 3rd edn (Oxford: Oxford University Press)

[19] Monakhov I, Bécoulet A, Fraboulet D and Nguyen F 1999 1D full wave treatment of mode conversion process at the ion–ion hybrid resonance in a bounded tokamak plasma *Phys. Plasmas* **6** 885

[20] Hasegawa A and Chen L 1976 Kinetic processes in plasma heating by resonant mode conversion of alfvén wave *Phys. Fluids* **19** 1924

[21] Majeski R, Phillips C K and Wilson J R 1994 Electron heating and current drive by mode converted slow waves *Phys. Rev. Lett.* **73** 2204

[22] Landau L D and Lifshitz E M 1977 *Quantum Mechanics (Non-relativistic Theory)* 3rd edn (Oxford: Pergamon Press)

[23] Akers R J *et al* 2002 Neutral beam heating in the START spherical tokamak *Nucl. Fusion* **42** 122